Stabilization of the Ferroelectric Phase in Epitaxial Hf 1− x Zr x O 2 Enabling Coexistence of Ferroelectric and Enhanced Piezoelectric Properties

Tingfeng Song, Huan Tan, Nico Dix, Rahma Moalla, Jike Lyu, Guillaume Saint-Girons, Romain Bachelet, Florencio Sánchez, Ignasi Fina

Stabilization of ferroelectric phase in epitaxial $Hf_{1-x}Zr_xO_2$ enabling coexistence of ferroelectric and enhanced piezoelectric properties

Tingfeng Song,[1] Huan Tan, [1] Nico Dix, [1] Rahma Moalla,[2] Guillaume Saint-Girons,[2] Romain Bachelet,[2] Florencio Sánchez,[1,] and Ignasi Fina,[1,*]*

[1]Institut de Ciència de Materials de Barcelona (ICMAB-CSIC), Campus UAB, E-08193 Bellaterra, Barcelona, Spain

[2]Institut des Nanotechnologies de Lyon (INL-CNRS UMR 5270), Université de Lyon, Ecole Centrale de Lyon, 36 avenue Guy de Collongue, 69134 Ecully Cedex, France.

Corresponding: ifina@icmab.es; fsanchez@icmab.es

Keywords:

hafnium oxide; ferroelectric; thin films; epitaxial oxides

Abstract

Systematic studies on polycrystalline $Hf_{1-x}Zr_xO_2$ films varying Zr content show that HfO_2 films are paraelectric (monoclinic). If Zr content is increased films become ferroelectric (orthorhombic) and after antiferroelectric (tetragonal). Whereas HfO_2 shows very good insulating properties and it is used in metal-oxide-semiconductor field-effect devices, ZrO_2 shows good piezoelectric properties, but it is antiferroelectric. In between, $Hf_{0.5}Zr_{0.5}O_2$ shows good ferroelectric properties at expenses of poorer insulating and piezoelectric properties than HfO_2 and ZrO_2, respectively. Here, we explore ferroelectric, insulating and piezoelectric properties of a series of epitaxial films of $Hf_{1-x}Zr_xO_2$ with different composition. We show that epitaxial growth enhances the stabilization of the ferroelectric behaviour compared with polycrystalline films in a wider compositional range and up to around 1000 K. This allows, in epitaxial ZrO_2 films ferroelectricity coexists with better piezoelectric and insulating properties than $Hf_{0.5}Zr_{0.5}O_2$ and in HfO_2 epitaxial films ferroelectricity coexists with better insulating properties than $Hf_{0.5}Zr_{0.5}O_2$. In both cases, the ferroelectric endurance is poorer than for $Hf_{0.5}Zr_{0.5}O_2$.

Introduction

The discovery of ferroelectricity and antiferroelectricity in $Hf_{1-x}Zr_xO_2$ (x=0-1) films, a material fully compatible with CMOS processes, is arising increasing interest for microelectronics in recent years.[1,2,3,4] The systematical investigation of polycrystalline $Hf_{1-x}Zr_xO_2$ (x=0-1) films grown by atomic layer deposition (ALD) shows that: i) in pure HfO_2 films the paraelectric centrosymmetric monoclinic phase (m-phase, $P2_1/c$) stabilizes, ii) in films with x near 0.5 the ferroelectric centrosymmetric orthorhombic phase (o-phase, $Pca2_1$) stabilizes and iii) in Zr-rich films tetragonal phase (t-phase, $P4_2/nmc$) stabilizes [2,5,6,7,8]. Whereas pure HfO_2 films, which are used as an ultrathin gate oxide in metal-oxide-semiconductor field-effect devices [9,10], show very good insulating properties and are paraelectric, the pure ZrO_2 films show good piezoelectric and insulating properties and are antiferroelectric [11,12]. In between, $Hf_{0.5}Zr_{0.5}O_2$ films show good ferroelectric properties which are promising for non-volatile memory devices and field effect transistors [3]. Thus in polycrystalline $Hf_{1-x}Zr_xO_2$ (x=0-1) films good insulating, ferroelectric and piezoelectric properties do not coexist for any x value. Specific studies on showing that HfO_2 films can also display ferroelectricity by annealing encapsulated devices, which requires of top electrode deposition in the amorphous state, as great as 10 $\mu C/cm^2$.[13] This value can be enhanced in reduced films at expenses of leakage increase.[14] Orthorhombic ferroelectric phase can be also stabilized in ZrO_2 films using several growth techniques showing remanent polarization values up to ≈ 50 $\mu C/cm^2$, with poor or not reported endurance.[11,12,15,16,17,18,2020-Huan] Better endurance is displayed by electrostatically engineered intrinsically antiferroelectric ZrO_2 films owing to the achievement of low coercive field.[19] However, there is a lack of studies focused on stabilized ferroelectric phase in a wider composition range and characterizing in detail phase stability and ferroelectric and piezoelectric properties.

Epitaxial ferroelectric $Hf_{0.5}Zr_{0.5}O_2$ films are of great interest to better understand the functional properties of the material, which is a challenge for polycrystalline films. Ferroelectric epitaxial $Hf_{0.5}Zr_{0.5}O_2$ films can be obtained by pulsed laser deposition (PLD). Epitaxial growth by PLD allows a good control of the different stable phases of $Hf_{0.5}Zr_{0.5}O_2$ by modifying the temperature and oxygen pressure control during deposition, film thickness, and by strain engineering [20,21,22,23,24,25,26,27,28]. Remarkably, endurance up to 10^{11} cycles without dielectric breakdown and retention longer than 10 years have been highlighted in sub-5 nm epitaxial $Hf_{0.5}Zr_{0.5}O_2$ films [29]. Investigations on epitaxial films with other Zr concentrations were scarcely reported.. $Hf_{1-x}Zr_xO_2$ films (x=0.5, 0.7 and 0.85) were grown epitaxially on Si(111) and Si(100) substrates, but in this case ferroelectricity was poor (saturation polarization below 2 $\mu C/cm^2$ at 10 K in the best sample) [27]. All in all, the effect of varying Zr concentration on epitaxial $Hf_{1-x}Zr_xO_2$ films has not been systematically investigated, which is critical for further understanding epitaxial films of HfO_2 and ZrO_2 system.

Here, we explore ferroelectric, insulating and piezoelectric properties of a series of 10 nm epitaxial films of $Hf_{1-x}Zr_xO_2$ with different composition (x=0, 0.25, 0.5, 0.75 and 1) on (001)-oriented $SrTiO_3$ (STO) substrates buffered with a $La_{2/3}Sr_{1/3}MnO_3$ (LSMO) electrode. We show that epitaxial growth enhances the stabilization of the ferroelectric orthorhombic phase for a broader compositional range compared with polycrystalline films. Orthorhombic phase is observed to be stable up to very high temperatures, above 1100 K for $Hf_{0.5}Zr_{0.5}O_2$, above to the ferroelectric to paraelectric phase transition in the 650-900 K range reported for other polycrystalline and epitaxial doped HfO_2 films.[32,33,34,35,36] Structural characterization indicates that the enhanced ferroelectricity results from the stabilization of orthorhombic phase in all the explored compositions. Therefore, in epitaxial films of larger Zr content ferroelectricity coexists with better piezoelectric and insulating properties than $Hf_{0.5}Zr_{0.5}O_2$ and in epitaxial films of larger Hf content ferroelectricity coexists with better insulating properties than $Hf_{0.5}Zr_{0.5}O_2$ films.

Results and discussions

Figure 1a shows XRD θ-2θ scans for all the films (see Supporting information S2 for wider scans). As shown in Figure 1a, the peaks around $2\theta \approx 30.1^o$, corresponding to orthorhombic (o) (111) reflection [20], can be clearly observed in all $Hf_{1-x}Zr_xO_2$ films. XRD 2θ-χ frames (Supporting information S2) show intense and narrow o(111) spots in all $Hf_{1-x}Zr_xO_2$ films, indicative of high texture. Further structural characterization in representative films reveals the existence of four (111)-oriented domains, rotated 90° with respect to each other (Supporting information S3). Diffraction peaks at ≈28.5° in Figure 1a signals the presence of monoclinic (m) phase (the peak corresponds to the m(-111) reflection) for x=0 and 0.25 films. When Zr content increases, the m(-111) peak gradually vanishes and only Laue fringes from o(111) peak are observed. Diffraction peaks at ≈34.5° in the x=0.25, 0.50, 0.75 and 1 films correspond to m/o{002} reflections. It needs to be noticed the possible overlapping of (101) reflection of tetragonal phase at ≈30.1° and of (002) reflection of tetragonal (t) phase at ≈ 34.5° with the described orthorhombic and monoclinic reflections, respectively. Previous transmission electron microscopy investigation in films nominally grown in the same conditions showed no presence of tetragonal phase in x=0.5 films, which disregards its significant presence in the studied films, [26] but not on films with greater Zr content.

The out-of-plane lattice parameter [$d_{o(111)}$] was extracted from the position of the o(111) reflection in the XRD θ-2θ scans (Figure 1a) and it is shown in Figure 1b. The $d_{o(111)}$ value gradually decreases (square symbols) from 2.978 Å to 2.959 Å while increasing Zr content, in agreement with results found in polycrystalline films [2]. The intensity of o(111) peak ($I_{o\text{-}HZO(111)}$, round symbols), normalized to that of LSMO(002) peak ($I_{LSMO(002)}$), reaches a maxima at x=0.5, then gradually decreasing. This indicates that the content of ferroelectric orthorhombic phase is greater in the x=0.5 film. The intensity of o(111) peak is greater for x=1 than for x=0, which indicates that the orthorhombic phase, maybe coexisting with the tetragonal, is more abundant in ZrO_2 film. Topographic images of $Hf_{1-x}Zr_xO_2$ films are shown in Supporting information S4,

revealing flat surface of all films with root-means-square (RSM) roughness below 0.4 nm.

Figure 1c shows polarization-voltage (P-V) loops for all films. It can be observed that all the loops show hysteresis with switchable remanent polarization. This is confirmed by the well-visible ferroelectric switching current peaks of intensity-voltage (I-V) loops (Supporting information S5) present in all the films, which univocally demonstrate their ferroelectric character. In figure 1d, it is plotted the dependence of the remanent polarization (P_r) with Zr content using dynamic leakage current compensation (DLCC) and positive up negative down (PUND) techniques for leakage subtraction. It is shown that the remanent polarization gradually increases with Zr content. Pure ZrO_2 film shows maximum $P_r \approx 27$ $\mu C/cm^2$ (Figure 1e), which is significant larger than that of equivalent epitaxial $Hf_{0.5}Zr_{0.5}O_2$ films of similar thickness. Density-functional calculations demonstrated that compressive epitaxial strain might favour the stabilization of ferroelectric o-phase in pure ZrO_2 films, rather than antiferroelectric t-phase, in agreement with the X-ray and ferroelectric characterization [37]. However, the fact that the films are not pure (with coexisting monoclinic or orthorhombic (001) phase as inferred from structural characterization) indicates that hysteresis in P-V loop of ZrO_2 results from coexisting switching mechanisms or extrinsic contributions. In fact, two current peaks appear in the I-V loops (Supporting information S5) at 3 and near 6 V. Note that the two peaks are both positive for positive applied voltage and negative for negative applied voltage, thus not related with the potential antiferroelectric character of the film.

Figure 2 summarizes XRD data as a function of increasing temperature for HfO_2, $Hf_{0.5}Zr_{0.5}O_2$ and ZrO_2 films (Supporting Information S6 includes raw data). In Figure 2a, 2θ-temperature diffraction map of the HfO_2 film is shown. It can be observed that, whereas the diffraction peak appearing at lower angles ascribed to the m(-111) reflection is observed up to 1100 K, the diffraction peak appearing at higher angles ascribed to the o(111) reflection disappears at above 1000 K. The integrated peaks intensity is plotted as a function of temperature in Figure 2b. It can be more clearly inferred that the o(111) intensity is constant up to 600 K when it starts to slightly decrease up to near 1000 K where it drops. Instead, the m(-111) intensity is nearly constant in the explored range. This indicates that monoclinic phase is stable in the whole temperature range and the orthorhombic ferroelectric phase is stable up to near 1000 K. In Figure 2c, 2θ-temperature diffraction map of the $Hf_{0.5}Zr_{0.5}O_2$ film is shown. It can be observed that in this case both o(111) and m(-111) reflections are present in all the explored temperature range. In Figure 2d, it can be observed that o(111) intensity gradually decreases with temperature, but any transition is not observed. The same absence of transition is observed in polycrystalline samples [2012 – Muller - NL]. The jump appearing at 700 K is ascribed to an experimental artifact also observed in the reflection belonging to the substrate. In Figure 2d, 2θ-temperature diffraction map of the ZrO_2 film is shown. Here, the monoclinic reflection is barely observed and the orthorhombic one is well-visible in all the explored temperature range. The integrated peak intensity of the o(111) reflection as a function of temperature is shown in Figure 2f. Again, a gradual decrease with temperature and absence of phase transition is observed.

In Figure 2 a,c,d, the shift towards lower angles of the diffraction peaks with temperature consequence of thermal expansion is also observed. The extracted thermal expansion coefficients (TEC) for the o(111) reflection are (Supporting Information S6) 5.5, 9.2 and 11.4 x10^{-6} 1/K for HfO_2, $Hf_{0.5}Zr_{0.5}O_2$ and ZrO_2 films, respectively. The absolute TEC value is largely influenced by the substrate presence, but it is STO(001) in all cases and thus it is worth noting that TEC increases with Zr content.

Figure 3a shows the piezoresponse force microscopy (PFM) loops recorded for x=0.5, 0.75 and 1. It can be observed that whereas ZrO_2 film shows sizable response, the $Hf_{0.5}Zr_{0.5}O_2$ film piezoelectric response is negligible under our experimental set-up sensitivity. In between the $Hf_{0.25}Zr_{0.75}O_2$ shows intermediate response with visible hysteresis but small amplitude. The coercive voltage for ZrO_2 (≈2V) is near the position of the low voltage ferroelectric switching peak in the I-V loop of Supporting Information S5 (≈3V). The difference between the coercive voltages is ascribed to the difference in the contact resistance using deposited Pt or the microscope conducting tip and the extremely different used frequency (1 Hz for PFM loop and 1 kHz for P-V loop), which can significantly affect the coercive field. [38] Figure 3b shows the current density versus applied voltage characteristics used to evaluate leakage current shown in Figure 3c. It can be observed that the leakage is the largest for the x=0.5 film. The extreme films, x=1 and x=0, show the lowest leakage current. Thus, ferroelectricity coexists with low leakage in pure ZrO_2 and HfO_2 samples, being the largest piezoelectric response for ZrO_2. The remarkable piezoelectric and low leakage current in ZrO_2 results from the enhanced stabilization of the orthorhombic phase in epitaxial films, and it cannot be found in polycrystalline samples in the pristine state. [11,12].

To further clarify the ferroelectric origin of the P-V loop hysteresis in Zr-rich films, PUND measurements were performed for ZrO_2 and $Hf_{0.5}Zr_{0.5}O_2$ films. PUND current versus voltage loop (Figure 4a) of $Hf_{0.5}Zr_{0.5}O_2$ film shows clearly distinguishable switching current peaks. The remanent polarization after subtraction is 18.1 $\mu C/cm^2$ (Supporting information S7) very near to the 19.8 $\mu C/cm^2$ obtained using DLCC mode (Figure 1c). Thus confirming the ferroelectric nature of the hysteretical polarization loop shown in figure 1c for this sample. PUND current versus voltage loop (Figure 4a) of ZrO_2 film shows two switching current peaks for both polarities (signalled by arrows). The integrated polarization is now 27 $\mu C/cm^2$ (Supporting information S7) also near to the 30.3 $\mu C/cm^2$ obtained using DLCC mode (Figure 1c). The PUND measurements for other samples are shown in Supporting information S7. These P_r values are near to those observed in sub-7 nm ZrO2 films [2020-Huan]. Thus, two switching contributions appear in DLCC and after PUND subtraction loops and these two switching contributions are reproducible in ZrO_2 films (see Supporting Information S8). The described PFM characterization allows us to safely conclude that the first current peak (at 3 V) can be ascribed to ferroelectric switching. The origin of the second current peak is difficult to disclose. Large resistive switching behaviour in ZrO_2 film due to ionic motion is known [39]. In fact, resistive switching characterization (see Supporting Information S9) shows that electroresistance (Figure 4b) in this film is

particularly large. Resistive switching due to its frequency dependence and hysteretic character cannot be completely suppressed using PUND and DLCC techniques. Thus although the ferroelectric character of the ZrO_2 film is confirmed, quantifying P_r is difficult due to the large electroresistance of this composition that contributes to the P-V loop measurement. For $Hf_{0.25}Zr_{0.75}O_2$ double peak is absent (Figure 4a). The remanent polarization after PUND subtraction is 25.6 $\mu C/cm^2$, in this case the evaluated electroresistance is not significantly larger than that shown in $Hf_{0.5}Zr_{0.5}O_2$ film. Thus, important extrinsic contributions can be disregarded indicating that $Hf_{0.25}Zr_{0.75}O_2$ shows large ferroelectric polarization coexisting with sizeable piezoelectric response.

The endurance characterization of epitaxial $Hf_{1-x}Zr_xO_2$ films is summarized in Figure 5. The memory window ($2P_r$) of $Hf_{1-x}Zr_xO_2$ films after different number of cycles (Figure 5a) indicates that there is not wake-up effect, and the pristine films possess the largest memory window, which is in contrast to polycrystalline $Hf_{1-x}Zr_xO_2$ films [6]. Similarly for ZrO_2 film, there is not wake-up effect, contrary to polycrystalline ZrO_2 films [11,12]. For this film, the memory window reduces from 32 $\mu C/cm^2$ to 15.2 $\mu C/cm^2$ after 10^4 cycles under electric field of 4.5 MV/cm, and capacitor breakdown occurs for further cycling. From I-V curves show in Figure 5b, it can be observed that both ferroelectric switching current peak (signaled by an arrow) are still present after 10^4 cycles. The fast breakdown of ZrO_2 films might result from the presence of important ionic conduction origin of the electroresistance already discussed. In addition, the larger piezoelectric response of ZrO_2 film can lead to rapid failure due to substrate clamping effect [40]. $Hf_{0.25}Zr_{0.75}O_2$ film is fatigued under 4.9 MV/cm, but retains $2P_r$ = 16 $\mu C/cm^2$ after 10^6 cycles before hard breakdown. The $Hf_{0.5}Zr_{0.5}O_2$ film shows the best endurance up to 10^9 cycles with cycling field of 4.4 MV/cm [21]. $Hf_{0.75}Zr_{0.25}O_2$ film and HfO_2 film were measured at 4.9 MV/cm and 6 MV/cm, and initial polarization window dropped from 9.2 $\mu C/cm^2$ and 7.1 $\mu C/cm^2$ to about 2 $\mu C/cm^2$ after 10^6 cycles, respectively, without hard breakdown. From I-V curves of the HfO_2 film show in Figure 5c, it can be observed that the ferroelectric switching current peak is very small after 10^6 cycles, and that the obtained 2 $\mu C/cm^2$ is overestimated due to residual leakage and series resistance contributions [41]. Thus, in the HfO_2 intrinsic ferroelectric fatigue mechanisms are limiting the device endurance, instead of hard breakdown, due to the lower leakage current in this film.

Conclusions

In conclusion, epitaxial growth enhances the stabilization of the ferroelectric orthorhombic phase in $Hf_{1-x}Zr_xO_2$ (x=0-1) up to around 1000 K . This leads to coexistence of ferroelectricity with good piezoelectric and insulating properties in epitaxial ZrO_2 and HfO_2 films, respectively. The absence of hard breakdown in epitaxial pure HfO_2 films indicates that further optimization might lead to good endurance. Besides, the complex coexistence between resistive switching, piezoelectricity and ferroelectric in Zr rich film, and their good control owing to epitaxial makes this composition ideal candidate to further investigate the interplay between these different phenomena.

Experimental section

Sample preparation. $Hf_{1-x}Zr_xO_2$ (x=0-1) films (t≈10 nm, Supporting information S1) and bottom LSMO electrodes (t=25 nm) were grown on STO(001) substrates in a single process by PLD using a KrF excimer laser. Five $Hf_{1-x}Zr_xO_2$ ceramic bulks with composition of HfO_2, $Hf_{0.75}Zr_{0.25}O_2$, $Hf_{0.5}Zr_{0.5}O_2$, $Hf_{0.25}Zr_{0.75}O_2$ and ZrO_2 were sintered as targets. $Hf_{1-x}Zr_xO_2$ films were deposited at substrate temperature (measured using a thermocouple inserted in the heater block) of T_s=800 °C with dynamic oxygen pressure of PO_2=0.1 mbar and a laser frequency of 2 Hz. The growth parameters for LSMO electrodes were 5 Hz of laser frequency, T_s=700 °C and PO_2=0.1 mbar. After deposition, the films were cooled to room temperature under an oxygen pressure of 0.2 mbar. Circular platinum top electrodes with 20 μm in diameter and 20 nm in thickness, were deposited by sputtering through stencil masks for electrical characterization (see sketch in the inset of Figure 1e). Exact electrodes size were measured after deposition.

Structural characterization. The crystal structure characterization of $Hf_{1-x}Zr_xO_2$ films was performed by X-ray diffraction (XRD) with Cu Kα radiation. θ-2θ scans were conducted using a Siemens D5000 diffractometer equipped with point detector, and 2θ-χ frames and Φ scans were recorded by a Bruker D8-Advance diffractometer equipped with 2D detector. ROMAIN: TXRD methods.

Morphological characterization. Surface topography was studied by atomic force microscopy (AFM) in dynamic mode.

Ferroelectric characterization. Ferroelectric polarization loops, current leakage, and endurance were tested at room temperature by connecting LSMO bottom electrode to the ground and biasing the top Pt contact. These were performed using an AixACCT TFAnalyser2000 platform. Ferroelectric polarization loops were obtained in dynamic leakage current compensation (DLCC) mode with a frequency of 1 kHz to reduce the leakage influence [42,43]. Endurance was evaluated using bipolar square pulses at the frequency of 100 kHz, and after cycling, the fatigued memory window was extracted by DLCC. PUND loops were also conducted. In the PUND technique [43,44] five voltage pulses were applied. The first was negative and prepolarized the sample to a negative state. The second and the third pulses were positive; the second (P) polarized the sample and therefore the measured current contained the FE and non-FE contribution, while the current during the third (U) pulse only contained the non-ferroelectric contributions. Therefore, their subtraction allows to obtain, in principle, only the ferroelectric contribution. The same principle applies for the fourth (N) and fifth pulses (D) for the negative state. All the loops were collected at the maximum possible applied voltage before breakdown.

PFM characterization. Piezoresponse force microscopy (PFM) measurements were performed with an MFP-3D ASYLUM RESEARCH microscope (Oxford Instrument Co.), using the AppNano silicon (n-type) cantilevers with Pt coating (ANSCM-PT-50). To achieve better sensitivity, the dual AC resonance tracking (DART) method was employed [45]. PFM voltage hysteresis loops were always performed at remanence, using a dwell time of 100 ms. Ferroelectric piezoresponse was evaluated by $PFM^{signal} = PFM^{amplitude} \cdot \sin(PFM^{phase})$. Due to the difficulties quantifying PFM response in DART, piezoelectric coefficient has not been

evaluated although all the measurements in all samples are done in the same conditions making them comparable.

Supplementary material

Supplementary

Aknowledgments

Financial support from the Spanish Ministerio de Ciencia e Innovación, through the "Severo Ochoa" FUNFUTURE (CEX2019-000917-S) and the MAT2017-85232-R (AEI/FEDER, EU), PID2019-107727RB-I00 (AEI/FEDER, EU), and MAT2015-73839-JIN projects, and from Generalitat de Catalunya (2017 SGR 1377) is acknowledged. IF acknowledges Ramón y Cajal contract RYC-2017-22531 andBeca Leonardo from fundación BBVA. TS and TS are financially supported by China Scholarship Council (CSC) with No. 201807000104 and ****, respectively. TS and HT work has been done as a part of their Ph.D. program in Materials Science at Universitat Autònoma de Barcelona.

References

(1) Böscke, T. S.; Müller, J.; Bräuhaus, D.; Schröder, U.; Böttger, U. Ferroelectricity in Hafnium Oxide Thin Films. *Appl. Phys. Lett.* **2011**, *99* (10), 102903.

(2) Müller, J.; Böscke, T. S.; Schröder, U.; Mueller, S.; Bräuhaus, D.; Böttger, U.; Frey, L.; Mikolajick, T. Ferroelectricity in Simple Binary ZrO_2 and HfO_2. *Nano Lett.* **2012**, *12* (8), 4318–4323.

(3) Mikolajick, T.; Slesazeck, S.; Park, M. H.; Schroeder, U. Ferroelectric Hafnium Oxide for Ferroelectric Random-Access Memories and Ferroelectric Field-Effect Transistors. *MRS Bull.* **2018**, *43* (5), 340–346.

(4) Park, M. H.; Lee, Y. H.; Kim, H. J.; Kim, Y. J.; Moon, T.; Kim, K. Do; Müller, J.; Kersch, A.; Schroeder, U.; Mikolajick, T.; Hwang, C. S. Ferroelectricity and Antiferroelectricity of Doped Thin HfO_2-Based Films. *Adv. Mater.*. **2015**, 1811–1831.

(5) Müller, J.; Böscke, T. S.; Bräuhaus, D.; Schröder, U.; Böttger, U.; Sundqvist, J.; Kcher, P.; Mikolajick, T.; Frey, L. Ferroelectric Zr0.5Hf0.5O2 Thin Films for Nonvolatile Memory Applications. *Appl. Phys. Lett.* **2011**, *99* (11), 2011–2014.

(6) Park, M. H.; Kim, H. J.; Kim, Y. J.; Lee, Y. H.; Moon, T.; Kim, K. Do; Hyun, S. D.; Fengler, F.; Schroeder, U.; Hwang, C. S. Effect of Zr Content on the Wake-Up Effect in Hf1-XZrxO2 Films. *ACS Appl. Mater. Interfaces*. **2016**, *8* (24),15466–15475.

(7) Park, M. H.; Lee, Y. H.; Kim, H. J.; Schenk, T.; Lee, W.; Kim, K. Do; Fengler, F. P. G.; Mikolajick, T.; Schroeder, U.; Hwang, C. S. Surface and Grain Boundary Energy as the Key Enabler of Ferroelectricity in Nanoscale Hafnia-Zirconia: A Comparison of Model and Experiment. *Nanoscale* **2017**, *9* (28), 9973–9986.

(8) Schenk, T.; Anspoks, A.; Jonane, I.; Ignatans, R.; Johnson, B. S.; Jones, J. L.; Tallarida, M.; Marini, C.; Simonelli, L.; Hönicke, P.; Richter, C.; Mikolajick, T.; Schroeder, U. Local Structural Investigation of Hafnia-Zirconia Polymorphs in Powders and Thin Films by X-Ray Absorption Spectroscopy. *Acta Mater.* **2019**, *180*, 158–169.

(9) Choi, J. H.; Mao, Y.; Chang, J. P. Development of Hafnium Based High-k Materials - A Review. *Mater. Sci. Eng. R Reports* **2011**, *72* (6), 97–136.

(10) Li, W.; Zhou, J.; Cai, S.; Yu, Z.; Zhang, J.; Fang, N.; Li, T.; Wu, Y.; Chen, T.; Xie, X.; Ma, H.; Yan, K.; Dai, N.; Wu, X.; Zhao, H.; Wang, Z.; He, D.; Pan, L.; Shi, Y.; Wang, P.; Chen, W.; Nagashio, K.; Duan, X.; Wang, X. Uniform and Ultrathin High-κ Gate Dielectrics for Two-Dimensional Electronic Devices. *Nat. Electron.* **2019**, *2* (12), 563–571.

(11) Starschich, S.; Schenk, T.; Schroeder, U.; Boettger, U. Ferroelectric and Piezoelectric Properties of Hf1-XZrxO2 and Pure ZrO_2 Films. *Appl. Phys. Lett.* **2017**, *110* (18), 2–7.

(12) Starschich, S.; Böttger, U. Doped ZrO_2 for Future Lead Free Piezoelectric Devices. *J. Appl. Phys.* **2018**, *123* (4).

(13) Polakowski, P.; Müller, J. Ferroelectricity in Undoped Hafnium Oxide. *Appl. Phys. Lett.* **2015**, *106* (23).

(14) Pal, A.; Narasimhan, V. K.; Weeks, S.; Littau, K.; Pramanik, D.; Chiang, T. Enhancing Ferroelectricity in Dopant-Free Hafnium Oxide. *Appl. Phys. Lett.* **2017**, *110* (2), 3–7.

(15) Shibayama, S.; Nishimura, T.; Migita, S.; Toriumi, A. Thermodynamic Control of Ferroelectric-Phase Formation in $Hf_xZr_{1-x}O_2$ and ZrO_2. *J. Appl. Phys.* **2018**, *124* (18), 0–7.

(16) Lin, B. T.; Lu, Y. W.; Shieh, J.; Chen, M. J. Induction of Ferroelectricity in Nanoscale ZrO_2 Thin Films on Pt Electrode without Post-Annealing. *J. Eur. Ceram. Soc.* **2017**, *37* (3), 1135–1139.

(17) Fan, Z.; Deng, J.; Wang, J.; Liu, Z.; Yang, P.; Xiao, J.; Yan, X.; Dong, Z.; Wang, J.; Chen, J. Ferroelectricity Emerging in Strained (111)-Textured ZrO_2 Thin Films. *Appl. Phys. Lett.* **2016**, *108* (1), 012906.

(18) Yi, S. H.; Lin, B. T.; Hsu, T. Y.; Shieh, J.; Chen, M. J. Modulation of Ferroelectricity and Antiferroelectricity of Nanoscale ZrO_2 Thin Films Using Ultrathin Interfacial Layers. *J. Eur. Ceram. Soc.* **2019**, *39* (14), 4038–4045.

(19) Pešić, M.; Hoffmann, M.; Richter, C.; Mikolajick, T.; Schroeder, U. Nonvolatile Random Access Memory and Energy Storage Based on Antiferroelectric Like Hysteresis in ZrO2. *Adv. Funct. Mater.* **2016**, *26* (41), 7486–7494.

(20) Lyu, J.; Fina, I.; Solanas, R.; Fontcuberta, J.; Sánchez, F. Growth Window of Ferroelectric Epitaxial Hf 0.5 Zr 0.5 O 2 Thin Films . *ACS Appl. Electron. Mater.* **2019**, *1* (2), 220–228.

(21) Lyu, J.; Fina, I.; Solanas, R.; Fontcuberta, J.; Sánchez, F. Robust Ferroelectricity in Epitaxial Hf1/2Zr1/2O2 Thin Films. *Appl. Phys. Lett.* **2018**, *113* (8).

(22) Lyu, J.; Fina, I.; Fontcuberta, J.; Sánchez, F. Epitaxial Integration on Si(001) of Ferroelectric Hf 0.5 Zr 0.5 O 2 Capacitors with High Retention and Endurance. *ACS Appl. Mater. Interfaces* **2019**, No. 001.

(23) Wei, Y.; Nukala, P.; Salverda, M.; Matzen, S.; Zhao, H. J.; Momand, J.; Everhardt, A. S.; Agnus, G.; Blake, G. R.; Lecoeur, P.; Kooi, B. J.; Íñiguez, J.; Dkhil, B.; Noheda, B. A Rhombohedral Ferroelectric Phase in Epitaxially Strained Hf 0.5 Zr 0.5 O 2 Thin Films. *Nat. Mater.* **2018**, *17* (12), 1095–1100.

(24) Li, T.; Zhang, N.; Sun, Z.; Xie, C.; Ye, M.; Mazumdar, S.; Shu, L.; Wang, Y.; Wang, D.; Chen, L.; Ke, S.; Huang, H. Epitaxial Ferroelectric Hf0.5Zr0.5O2 Thin Film on a Buffered YSZ Substrate through Interface Reaction. *J. Mater. Chem. C* **2018**, *6* (34), 9224–9231.

(25) Lyu, J.; Fina, I.; Bachelet, R.; Saint-Girons, G.; Estandía, S.; Gázquez, J.; Fontcuberta, J.; Sánchez, F. Enhanced Ferroelectricity in Epitaxial Hf0.5Zr0.5O2 Thin Films Integrated with Si(001) Using SrTiO3 Templates. *Appl. Phys. Lett.* **2019**, *114* (22), 0–5.

(26) Estandía, S.; Dix, N.; Gazquez, J.; Fina, I.; Lyu, J.; Chisholm, M. F.; Fontcuberta, J.; Sánchez, F. Engineering Ferroelectric $Hf_{0.5}Zr_{0.5}O_2$ Thin Films by Epitaxial Stress . *ACS Appl. Electron. Mater.* **2019**, *1* (8), 1449–1457.

(27) Nukala, P.; Antoja-Lleonart, J.; Wei, Y.; Yedra, L.; Dkhil, B.; Noheda, B. Direct Epitaxial Growth of Polar $(1–x)HfO_2–(x)ZrO_2$ Ultrathin Films on Silicon. *ACS Appl. Electron. Mater.* **2019**, *1* (12), 2585–2593.

(28) Yoong, H. Y.; Wu, H.; Zhao, J.; Wang, H.; Guo, R.; Xiao, J.; Zhang, B.; Yang, P.; Pennycook, S. J.; Deng, N.; Yan, X.; Chen, J. Epitaxial Ferroelectric Hf0.5Zr0.5O2 Thin Films and Their Implementations in Memristors for Brain-Inspired Computing. *Adv. Funct. Mater.* **2018**, *28* (50), 1806037.

(29) Goh, Y.; Cho, S. H.; Park, S. H. K.; Jeon, S. Oxygen Vacancy Control as a Strategy to Achieve Highly Reliable Hafnia Ferroelectrics Using Oxide Electrode. *Nanoscale* **2020**, *12* (16), 9024–9031.

(30) Cheema, S. S.; Kwon, D.; Shanker, N.; dos Reis, R.; Hsu, S. L.; Xiao, J.; Zhang, H.; Wagner, R.; Datar, A.; McCarter, M. R.; Serrao, C. R.; Yadav, A. K.; Karbasian, G.; Hsu, C. H.; Tan, A. J.; Wang, L. C.; Thakare, V.; Zhang, X.; Mehta, A.; Karapetrova, E.; Chopdekar, R. V.; Shafer, P.; Arenholz, E.; Hu, C.; Proksch, R.; Ramesh, R.; Ciston, J.; Salahuddin, S. Enhanced Ferroelectricity in Ultrathin Films Grown Directly on Silicon. *Nature* **2020**, *580* (7804), 478–482.

(31) Choi, S.; Shiraishi, T.; Kiguchi, T.; Shimizu, T.; Funakubo, H.; Konno, T. J.

Formation of Polar Phase in Fe-Doped ZrO 2 Epitaxial Thin Films. *Appl. Phys. Lett.* **2018**, *113* (26), 2–7.

(32) Park, M. H.; Chung, C.-C.; Schenk, T.; Richter, C.; Hoffmann, M.; Wirth, S.; Jones, J. L.; Mikolajick, T.; Schroeder, U. Origin of Temperature-Dependent Ferroelectricity in Si-Doped HfO2. *Adv. Electron. Mater.* **2018**, *4* (4), 1700489.

(33) Shimizu, T.; Katayama, K.; Kiguchi, T.; Akama, A.; Konno, T. J.; Sakata, O.; Funakubo, H. The Demonstration of Significant Ferroelectricity in Epitaxial Y-Doped HfO2 Film. *Sci. Rep.* **2016**, *6* (September), 1–8.

(34) Shiraishi, T.; Choi, S.; Kiguchi, T.; Shimizu, T.; Uchida, H.; Funakubo, H.; Konno, T. J. Fabrication of Ferroelectric Fe Doped HfO2 Epitaxial Thin Films by Ion-Beam Sputtering Method and Their Characterization. *Jpn. J. Appl. Phys.* **2018**, *57* (11), 0–5.

(35) Mimura, T.; Shimizu, T.; Katsuya, Y.; Sakata, O.; Funakubo, H. Thickness- And Orientation- Dependences of Curie Temperature in Ferroelectric Epitaxial y Doped HfO2 Films. *Jpn. J. Appl. Phys.* **2020**, *59* (SG), 0–6.

(36) Shimizu, T.; Katayama, K.; Kiguchi, T.; Akama, A.; Konno, T. J.; Funakubo, H. Growth of Epitaxial Orthorhombic YO1.5-Substituted HfO2 Thin Film. *Appl. Phys. Lett.* **2015**, *107* (3), 232905.

(37) Reyes-Lillo, S. E.; Garrity, K. F.; Rabe, K. M. Antiferroelectricity in Thin-Film ZrO_2 from First Principles. *Phys. Rev. B* **2014**, *90* (14), 140103.

(38) Scott, J. F. Models for the Frequency Dependence of Coercive Field and the Size Dependence of Remanent Polarization in Ferroelectric Thin Films. *Integr. Ferroelectr.* **1996**, *12* (2–4), 71–81.

(39) Wu, X.; Zhou, P.; Li, J.; Chen, L. Y.; Lv, H. B.; Lin, Y. Y.; Tang, T. A. Reproducible Unipolar Resistance Switching in Stoichiometric ZrO2 Films. *Appl. Phys. Lett.* **2007**, *90* (18), 183507.

(40) Ahmad, M. Al; Coccetti, F.; Plana, R. The Effect of Substrate Clamping on Piezoelectric Thin-Film Parameters. In *2007 Asia-Pacific Microwave Conference*; **2007**, 1–4.

(41) González-Casal, S.; Fina, I.; Sánchez, F.; Fontcuberta, J. Direct Reversible Magnetoelectric Coupling in a Ferroelectric/Ferromagnetic Structure Controlled by Series Resistance Engineering. *ACS Appl. Electron. Mater*. **2019**, *1* (9), 1937–1944.

(42) Meyer, R.; Liedtke, R.; Waser, R. Oxygen Vacancy Migration and Time-Dependent Leakage Current Behavior of Ba0.3Sr0.7TiO3 Thin Films. *Appl. Phys. Lett.* **2005**, *86* (11), 1–3.

(43) Fina, I.; Fábrega, L.; Langenberg, E.; Mart, X.; Sánchez, F.; Varela, M.; Fontcuberta, J. Nonferroelectric Contributions to the Hysteresis Cycles in Manganite Thin Films: A Comparative Study of Measurement Techniques. *J. Appl. Phys.* **2011**, *109* (7), 0–6.

(44) Scott, J. F.; Kammerdiner, L.; Parris, M.; Traynor, S.; Ottenbacher, V.; Shawabkeh, A.; Oliver, W. F. Switching Kinetics of Lead Zirconate Titanate Submicron Thin-Film Memories. *J. Appl. Phys.* **1988**, *64* (2), 787–792.

(45) Rodriguez, B. J.; Callahan, C.; Kalinin, S. V.; Proksch, R. Dual-Frequency Resonance-Tracking Atomic Force Microscopy. *Nanotechnology* **2007**, *18* (47), 475504.

Figure 1

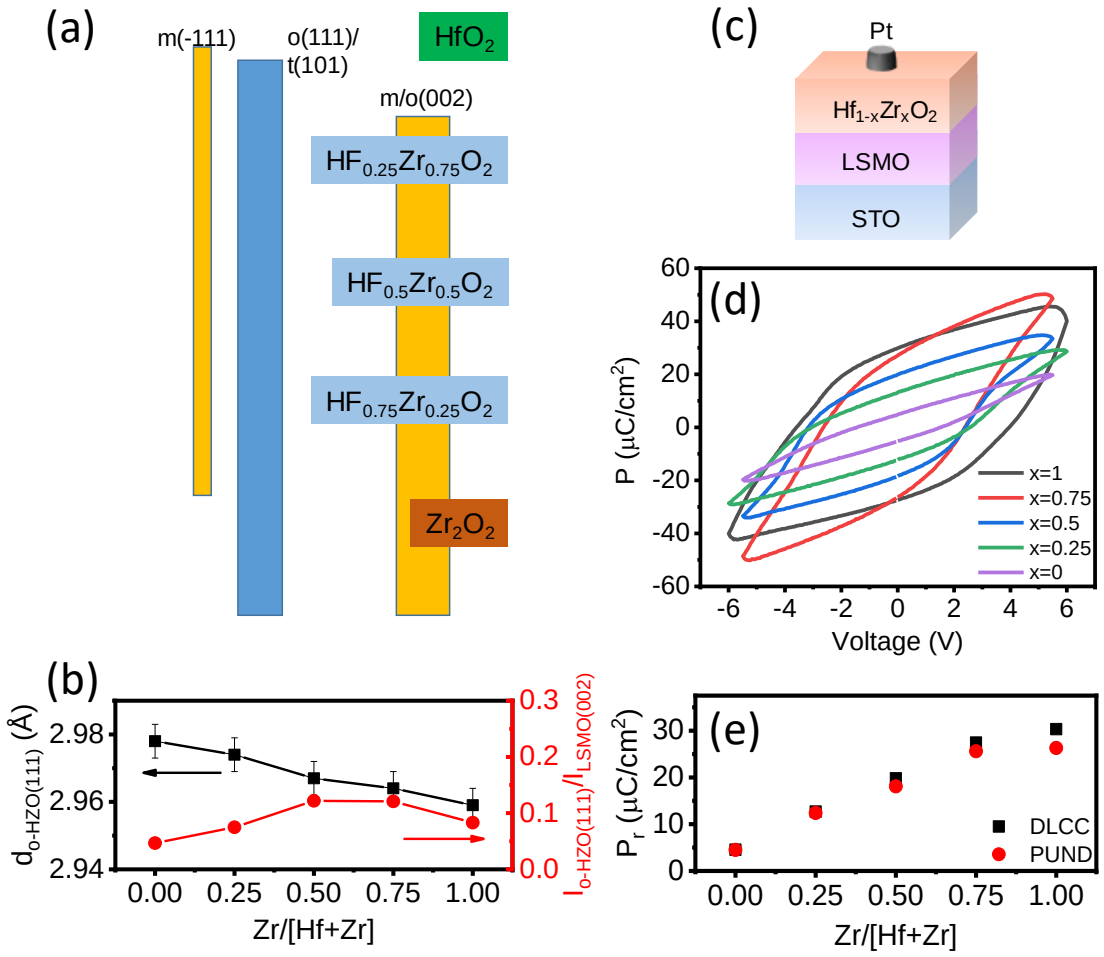

Figure 1. (a) XRD θ-2θ scans of $Hf_{1-x}Zr_xO_2$ films (x=0, 0.25, 0.5, 0.75 and 1). (b) Out-of-plane o-HZO(111) lattice distance of $Hf_{1-x}Zr_xO_2$ films (black squares) and intensity of o-HZO(111) normalized to LSMO(002) (red cycles), plotted as a function of Zr content. (c) Hysteresis loops of $Hf_{1-x}Zr_xO_2$ films. (d) Dependence of P_r on Zr content, recorded by DLCC (black squares) and PUND (red cycles) mode.

Figure 2

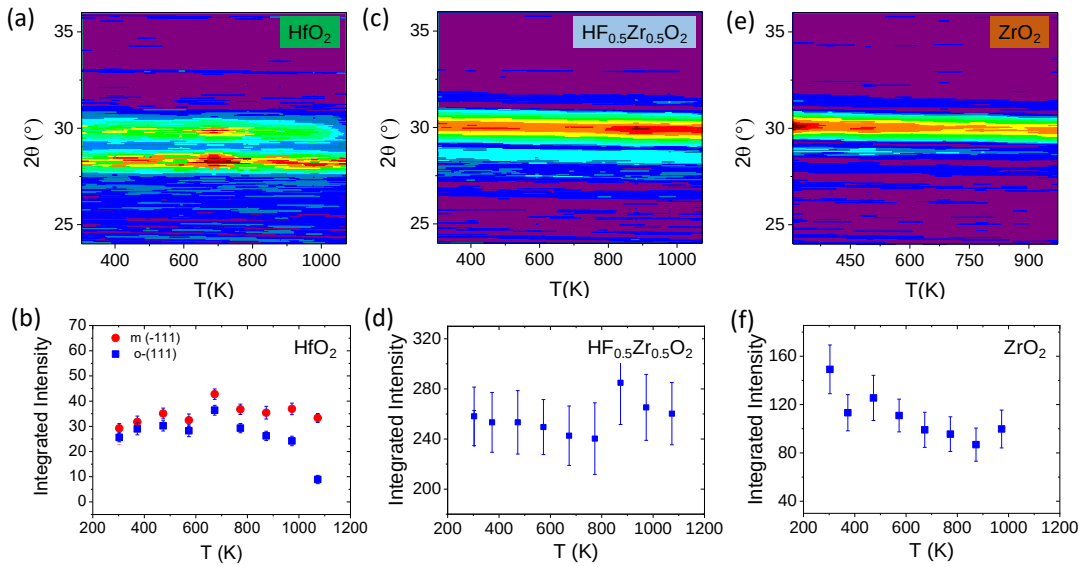

Figure 2. 2θ-temperature diffraction maps for $Hf_{1-x}Zr_xO_2$ x=0 (a), 0.5 (c) and 1 (d) films. The corresponding integrated intensity as a function of temperature for the o(111) peak is in panels (b,d,f). Panel b includes the temperature dependence of the intensity of the m(-111).

Figure 3

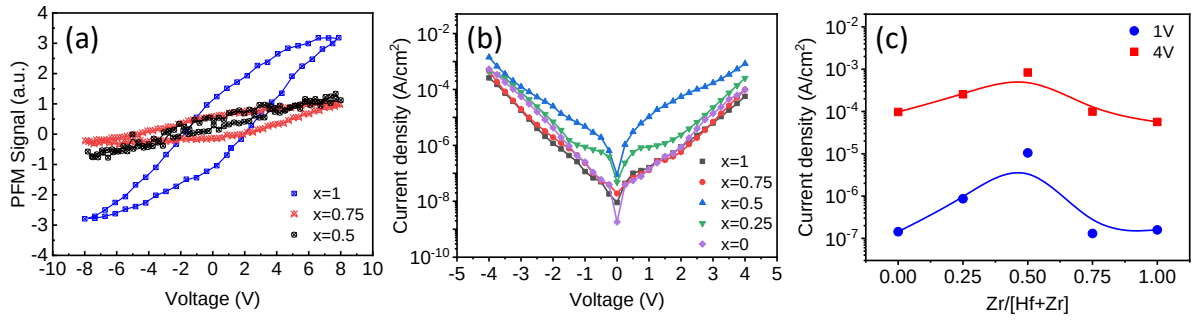

Figure 3. (a) PFM amplitude hysteresis loops taken on the bare surface of $Hf_{1-x}Zr_xO_2$ films (x=0.5, 0.75 and 1). (b) Current density versus applied voltage characteristics of all $Hf_{1-x}Zr_xO_2$ films. (c) Current density versus Zr content evaluated at 1 and 4 V.

Figure 4

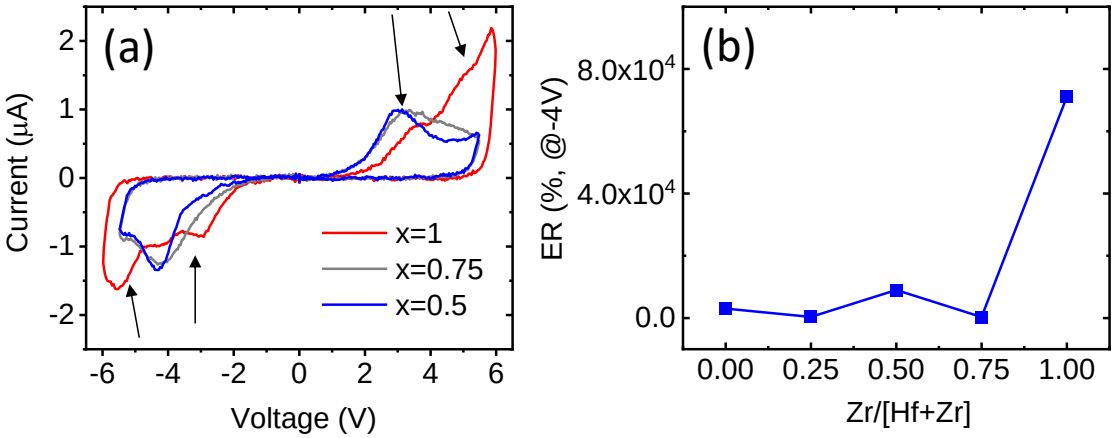

Figure 4. (a) Current versus voltage loops using PUND measurements of ZrO_2, $Hf_{0.25}Zr_{0.75}O_2$ and $Hf_{0.5}Zr_{0.5}O_2$ films recorded at 1kHz. (b) Electroresistance of $Hf_{1-x}Zr_xO_2$ films evaluated at -4V (see Supporting Information S8).

Figure 5

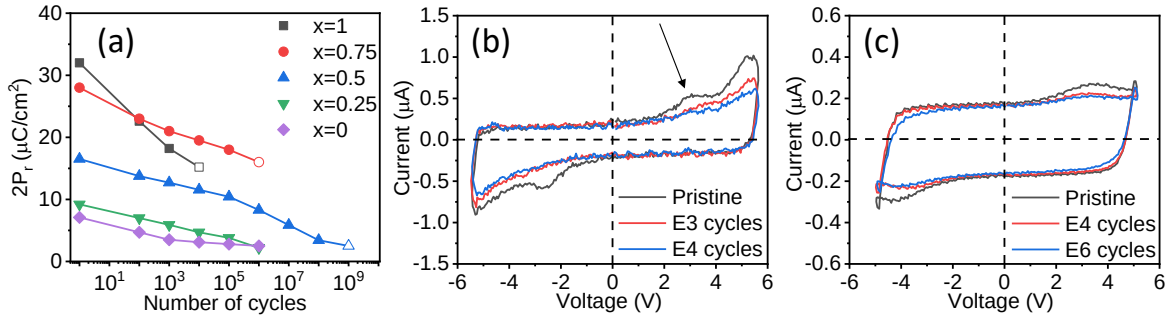

Figure 5. (a) The memory window ($2P_r$) of $Hf_{1-x}Zr_xO_2$ films after different number of cycles. Current-voltage curves of (b) ZrO_2 and (c) HfO_2 films after different number of cycles.

Supplementary material

Stabilization of ferroelectric phase in epitaxial $Hf_{1-x}Zr_xO_2$ enabling coexistence of ferroelectric and enhanced piezoelectric properties

Tingfeng Song,[1] Huan Tan, [1] Nico Dix, [1] Rahma Moalla,[2] Guillaume Saint-Girons,[2] Romain Bachelet,[2] Florencio Sánchez, [1] and Ignasi Fina[1]

[1]Institut de Ciència de Materials de Barcelona (ICMAB-CSIC), Campus UAB, E-08193 Bellaterra, Barcelona, Spain

[2]Institut des Nanotechnologies de Lyon (INL-CNRS UMR 5270), Université de Lyon, Ecole Centrale de Lyon, 36 avenue Guy de Collongue, 69134 Ecully Cedex, France.

Faltan los *

Supplementary material S1: simulation of Laue oscillations.

Figure S1(a-e) shows the X-ray diffraction (XRD) θ-2θ scans of the $Hf_{1-x}Zr_xO_2$ films on STO(001). The o-HZO(111) reflection is simulated (red curves) according to the equation [1]:

$$I(Q) = \left(\frac{\sin\left(\frac{QNc}{2}\right)}{\sin\left(\frac{Qc}{2}\right)} \right)^2$$

where $Q=4\pi\sin(\theta)/\lambda$ is the reciprocal space vector, N the number of unit cells along the out-of-plane direction and c the corresponding lattice parameter. The estimated thickness (black circles) and growth rate (blue squares) is shown in Figure S1-f. Slightly dependence on composition can be observed.

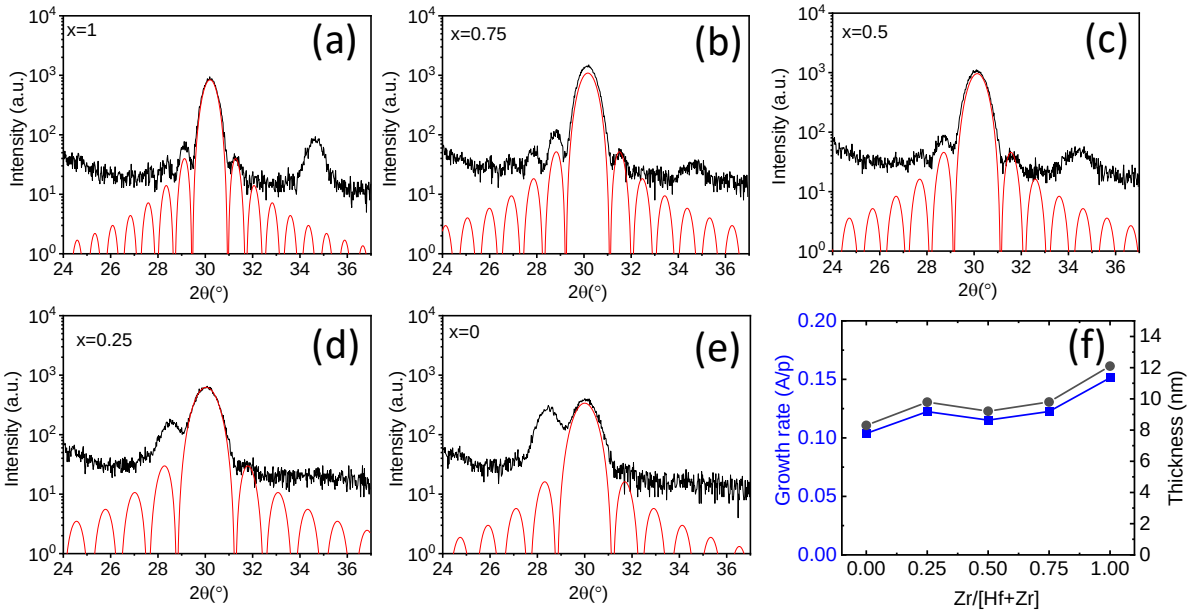

Figure S1. (a-e) XRD θ-2θ scans and (f) the estimated thickness (black circles) and growth rate (blue squares) of $Hf_{1-x}Zr_xO_2$ films on LSMO/STO(001). Red curves are simulations of Laue oscillations.

Supplementary material S2: XRD θ-2θ scans and 2θ-χ frames

The XRD θ-2θ scans show (001) reflections of STO and LSMO, and diffraction peaks in the 2θ range of 26-37° related to $Hf_xZr_{1-x}O_2$ (x=0-1) films. The peaks around 2θ=30.1°, corresponding to polar orthorhombic (111) phase, can be clearly observed in all samples. XRD 2θ-χ frames show bright circular spots corresponding to the STO substrate, the LSMO electrode, and the o(111) reflection. The narrow spot around χ=0° signals epitaxial ordering. In pure HfO_2 film, only o(111) and m(-111) reflections are observed.

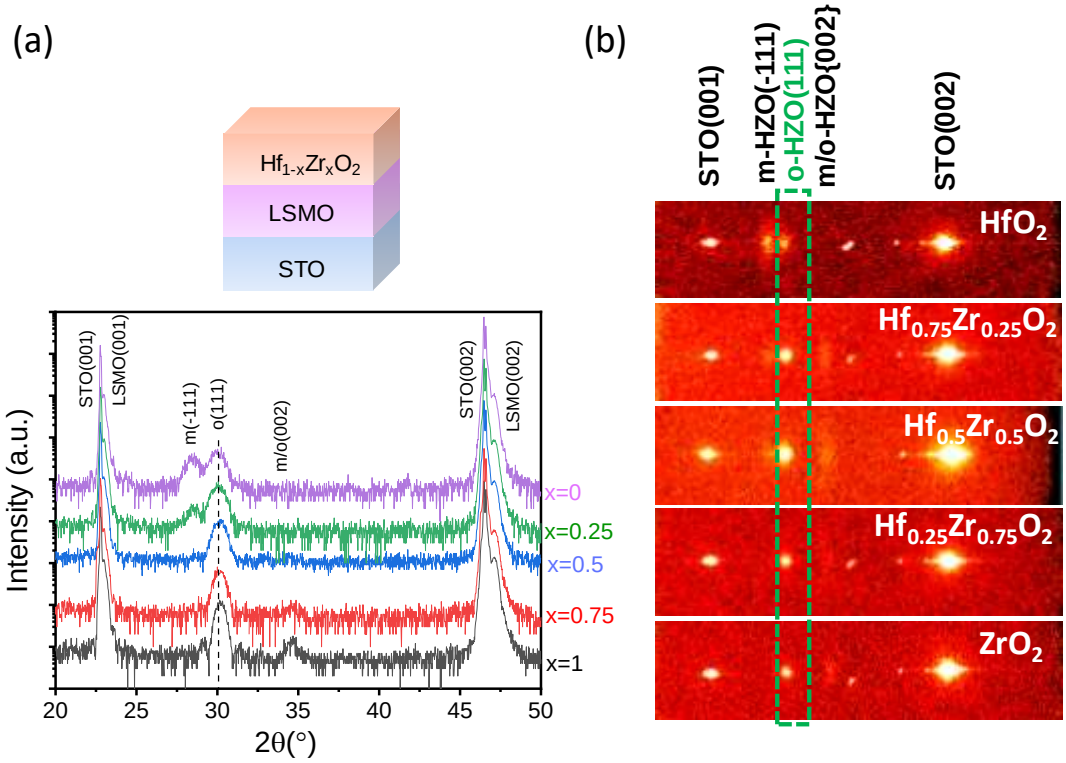

Figure S2. (a) XRD θ-2θ scans and (b) XRD 2θ-χ frames of $Hf_{1-x}Zr_xO_2$ films. Dashed green line rectangle mark the position of the o-HZO(111) reflection.

Supplementary material S3: XRD pole figures of ZrO_2 and $Hf_{0.5}Zr_{0.5}O_2$ films

Pole figures of ZrO_2 (a) and $Hf_{0.5}Zr_{0.5}O_2$ (b) films were conducted around (-111) to confirm the epitaxial characteristic. As indicated in the pole figures, 12 peaks , at an angle (χ) of ~71°, of o(-111) family reveal the existence of four in-plane crystal variants. The four peaks at χ around 55°, reveal the (001)-oriented phase in both ZrO_2 and $Hf_{0.5}Zr_{0.5}O_2$ films. The integrated 2θ-χ slices around the (001)-oriented phase are shown in figure (c) ZrO_2 and (d) $Hf_{0.5}Zr_{0.5}O_2$. In $Hf_{0.5}Zr_{0.5}O_2$ film, the three spots in the χ range from 50-60°, m(-111), m(111) and o(111)/t(001), indicate the formation of monoclinic phase. However, in pure ZrO_2 film, only one bright spot, o(111)/t(001), is observed in this range, indicating that the (001)-oriented phase is mainly composed of orthorhombic/tetragonal phase.

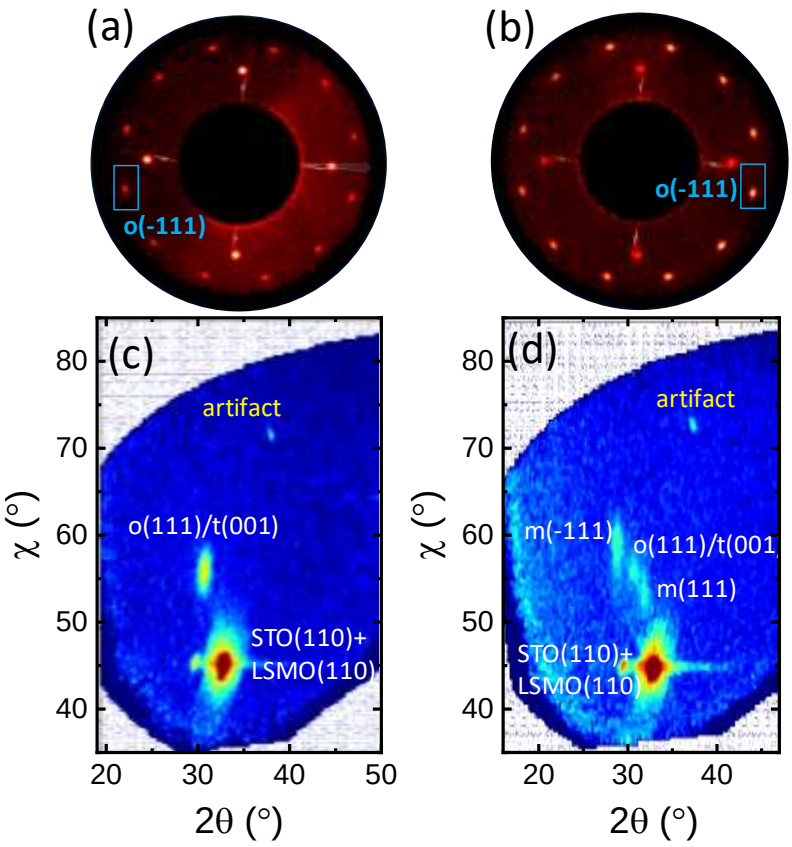

Figure S3. XRD pole figures of (a) ZrO_2 and (b) $Hf_{0.5}Zr_{0.5}O_2$ films. The integrated 2θ-χ slices around the (001)-oriented phase of (c) ZrO_2 and (d) $Hf_{0.5}Zr_{0.5}O_2$ films.

Supplementary material S4: topographic AFM images

Figure S4 shows topographic atomic force microscopy (AFM) images and height profiles of the $Hf_{1-x}Zr_xO_2$ films. The films are very flat, with a RSM roughness less than 0.42 nm. Morphology of terraces and steps is appreciated.

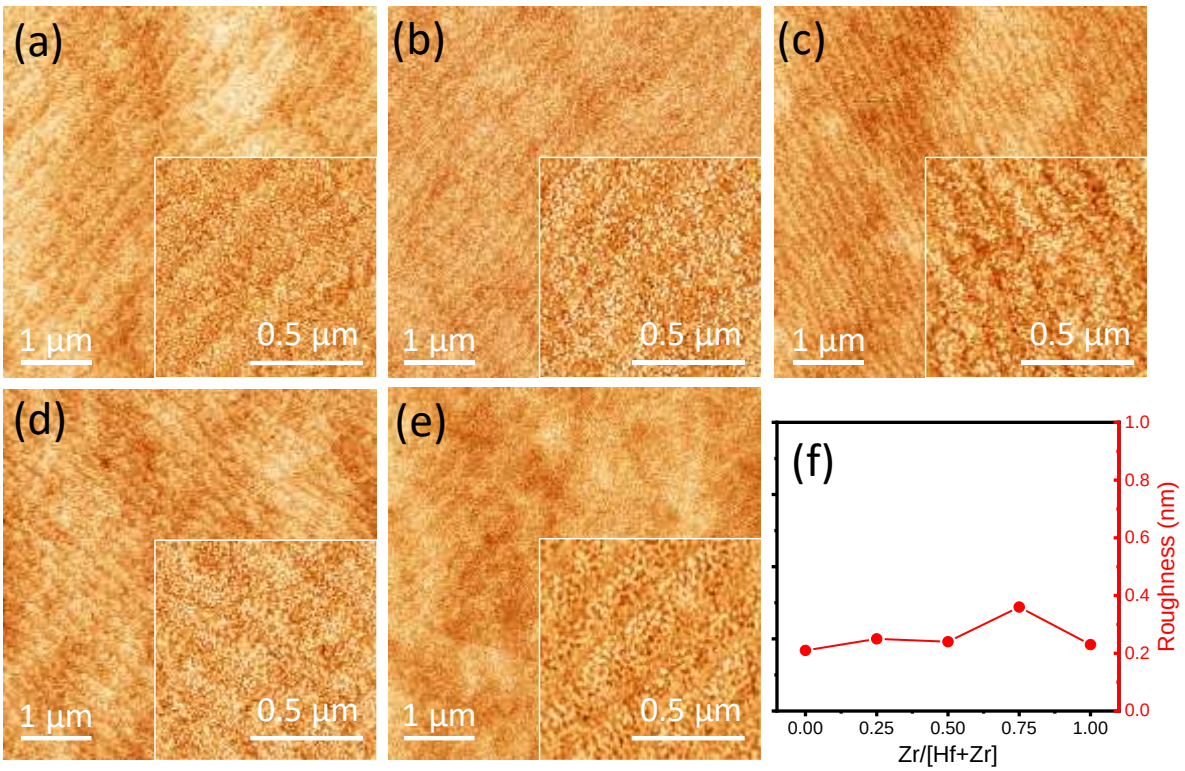

Figure S4. (a-e) Topographic AFM images, 5 µm x 5 µm, of the $Hf_{1-x}Zr_xO_2$ films. The inset in each image is a 1 µm x 1 µm scanned area. (f) summarized roughness (in 5 µm x 5 µm scanned areas) of films with different Zr content.

Supplementary material S5: P-V loops at increasing voltage

Figure S5 shows polarization and current versus voltage loops of $Hf_{1-x}Zr_xO_2$ (x=0-1) epitaxial films, measured at increasing voltage.

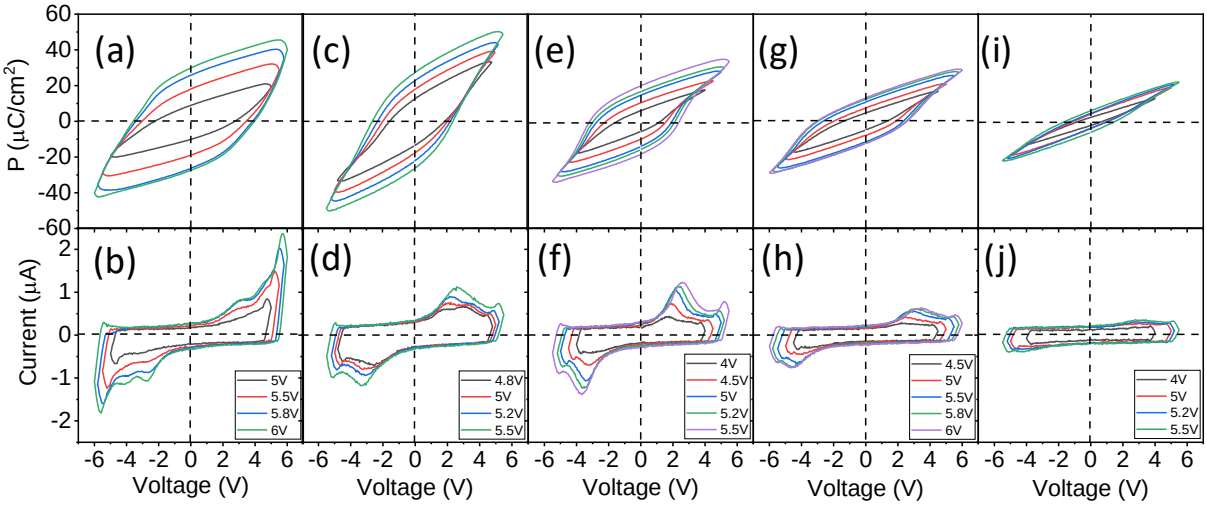

Figure S5. Polarization loops and corresponding current-voltage loops, measured at increasing voltage, of $Hf_{1-x}Zr_xO_2$ films, (a-b) x =1, (c-d) x =0.75, (e-f) x =0.5, (g-h) x =0.25 and (i-j) x =0.

Supplementary material S6: High temperature XRD scans for HfO_2, $Hf_{0.5}Zr_{0.5}O_2$ and ZrO_2 films.

Fig S6 shows the XRD 2θ data at increasing temperature for epitaxial HfO_2 (a), $Hf_{0.5}Zr_{0.5}O_2$ (b) and ZrO_2 (c) films. For pure HfO_2, the m(-111), around 28.5°, exists at the whole temperature range from 303K to 1073K. The intensity of o(111), around 30°, is gradually dropping with temperature increase. Both in $Hf_{0.5}Zr_{0.5}O_2$ and ZrO_2 films, o(111) can be stabled around 1000K. The relative inter-plannar spacing change with temperature is indicated in Fig S6(d-f). For HfO_2 film, the extracted thermal expansion coefficients (TEC) of the m(-111) and o(111) reflection are 3.35 and $5.5x10^{-6}$ 1/K, respectively. Based on the linear fitting, TEC of the o(111) reflection are 9.2 and 11.4 $x10^{-6}$ 1/K for $Hf_{0.5}Zr_{0.5}O_2$ and ZrO_2 films, respectively. It is worth noting that the absolute TEC value could be affected by the substrate.

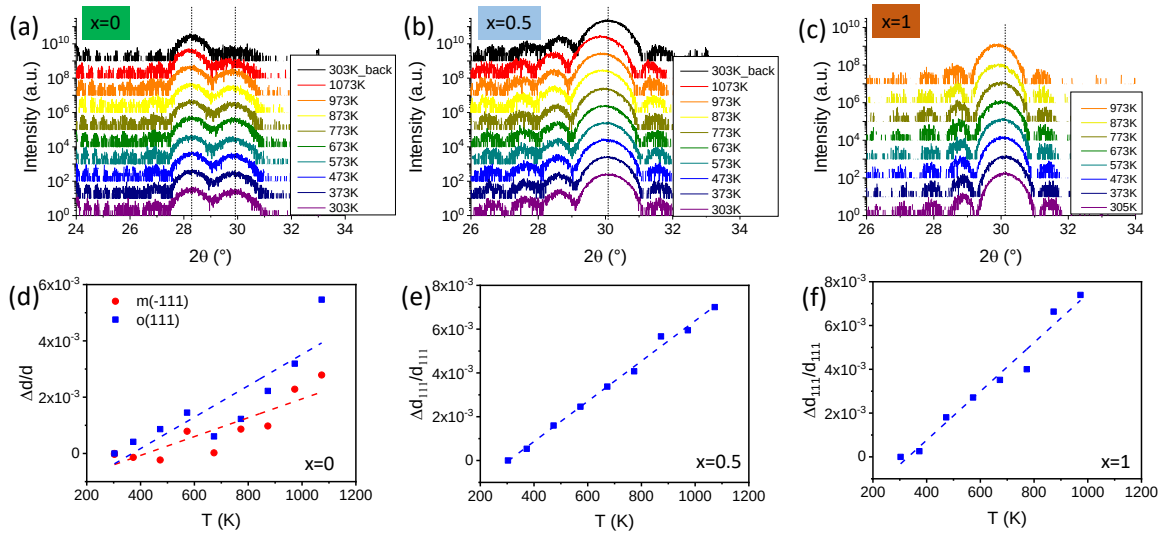

Figure S6. The XRD 2θ data with increasing temperature for (a) HfO_2, (c) $Hf_{0.5}Zr_{0.5}O_2$ and (e) ZrO_2 films. The extracted relative inter-plannar spacing change with temperature of (d) m(-111) and o(111) plane in HfO_2, and o(111) plane in (e) $Hf_{0.5}Zr_{0.5}O_2$ and (f) ZrO_2 films

Supplementary material S7: PUND loops $Hf_{1-x}Zr_xO_2$ epitaxial films

Figure S7 shows (a) current versus voltage and (b) polarization loops of $Hf_{1-x}Zr_xO_2$ (x =0-1) epitaxial films, measured using PUND.

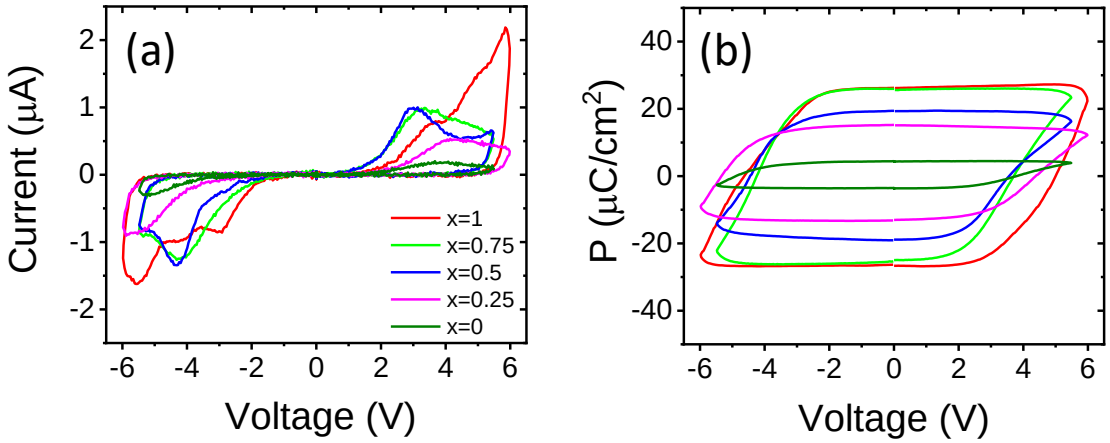

Figure S7. (a) Current and (b) polarization versus voltage loops, measured by PUND at 1 kHz, of $Hf_{1-x}Zr_xO_2$ (x =0-1) epitaxial films.

Supplementary material S8: PUND loops ZrO_2 epitaxial films

Figure S8 confirms the presence of the double switching ferroelectric peak in a second equivalent ZrO_2 film grown in another deposition process.

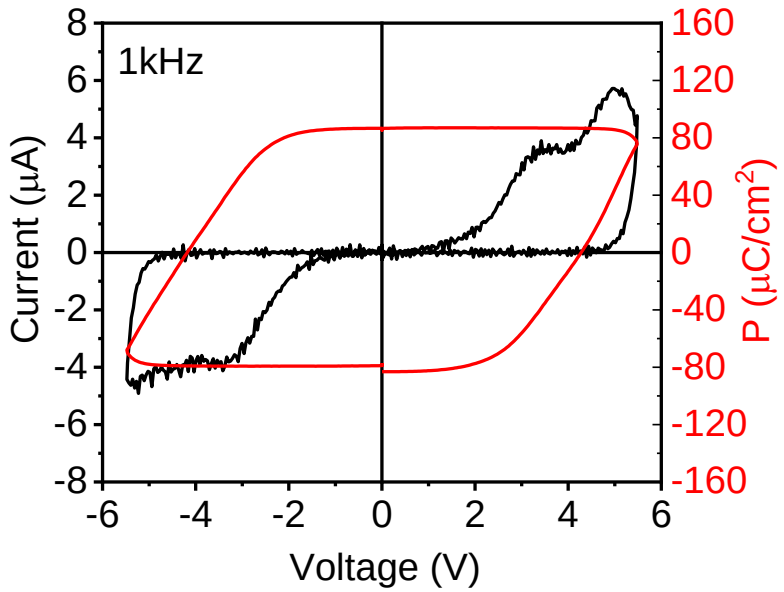

Figure S8. Current and polarization versus voltage loop using PUND measurement (1 kHz) of an ZrO_2 film grown in a different deposition process that the equivalent sample described in the manuscript.

Supplementary material S9: Resistive switching characterization of $Hf_{1-x}Zr_xO_2$ (x = 1, 0.75, 0.5, 0.25 and 0) epitaxial films

Figure S9 shows resistive switching characterization of $Hf_{1-x}Zr_xO_2$ (x =1, 0.75, 0.5, 0.25 and 0) epitaxial films, performed by applying a step shaped voltage waveform to the films and measuring the current response by the virtual ground amplifier at pristine state. Integration time for each data point is 2 s.

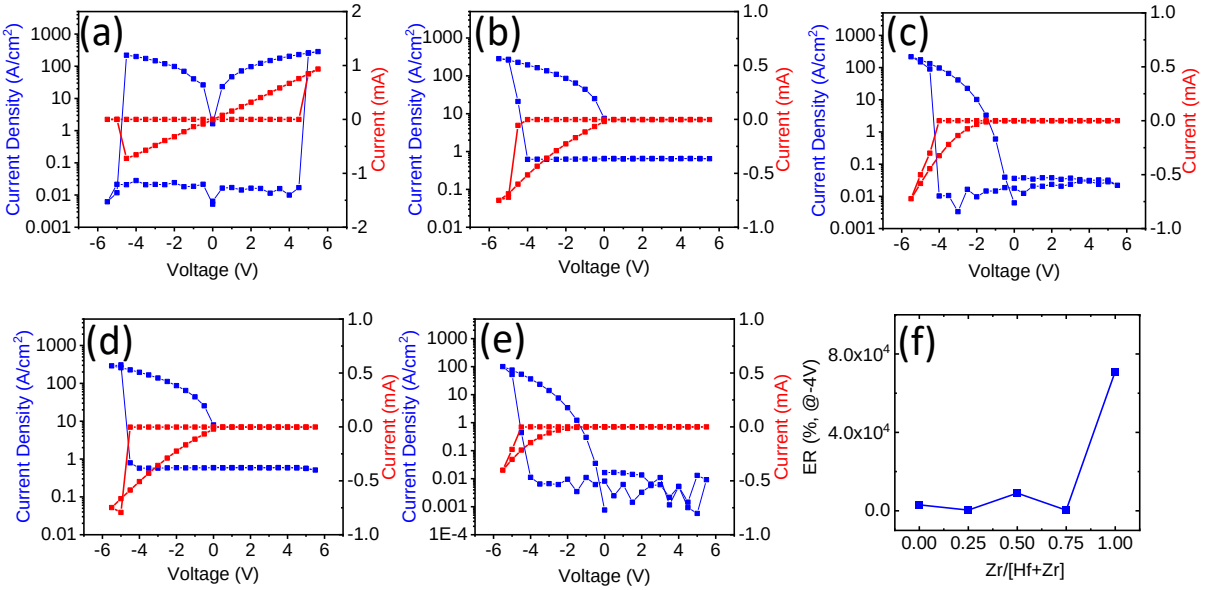

Figure S9. Current density and corresponding current versus voltage loops of $Hf_{1-x}Zr_xO_2$ epitaxial films, (a) x =1, (b) x =0.75, (c) x =0.5, (d) x =0.25 and (e) x =0. (f) Electroresistance of $Hf_{1-x}Zr_xO_2$ films evaluated at -4V.

Supplementary material References

[1] Lyu, J.; Fina, I.; Solanas, R.; Fontcuberta, J.; Sánchez, F. Robust Ferroelectricity in Epitaxial Hf1/2Zr1/2O2 Thin Films. *Appl. Phys. Lett.* **2018**, *113* (8).